J. Fluid Mech. (1978), *vol.* 84, *part* 3, *pp.* 561–580
Printed in Great Britain

Structure functions of temperature fluctuations in turbulent shear flows

By R. A. ANTONIA

Department of Mechanical Engineering, University of Newcastle, New South Wales 2308, Australia

AND C. W. VAN ATTA

Department of Applied Mechanics and Engineering Sciences, University of California, San Diego

(Received 20 October 1976 and in revised form 17 June 1977)

Structure functions of turbulent temperature and velocity fluctuations are measured both for the atmosphere, in the surface layer over land, and for the laboratory, in the inner region of a thermal boundary layer and on the axis of a heated jet. Even-order temperature structure functions, up to order eight, generally compare favourably with the analysis of Antonia & Van Atta over the inertial subrange. The Reynolds number dependence of these structure functions, as predicted by the analysis, is in qualitative agreement with the measured data. Odd-order temperature structure functions depart significantly from the isotropic value of zero, particularly at large time delays. This departure is reasonably well predicted, over the inertial subrange, by postulating a simple ramp model for the temperature fluctuations. Assumptions involved in this model are directly tested by measurements in the heated jet. The ramp structure does not seriously affect either the even-order temperature structure functions or the mixed velocity–temperature functions, which include even-order moments of the temperature difference.

1. Introduction

In a previous paper (Antonia & Van Atta 1975) an analysis based on dimensional arguments was developed to determine the behaviour of structure functions of velocity and temperature fluctuations in the inertial subrange. This analysis included the correlation between the dissipation fields of velocity and temperature fluctuations. Although this correlation was measured in a turbulent heated jet, no measurements of structure functions were made for direct comparison with the analytical expressions.

In this paper, we present measurements of the nth-order (with n as large as eight) structure functions of velocity and temperature fluctuations in various heated turbulent flows over a relatively large range of Reynolds numbers. The measured temperature structure functions are compared with measurements by Park (1976) in the atmospheric boundary layer above the surface of the ocean and with some earlier results obtained by Yeh (1971) in very low Reynolds number grid turbulence. The dependence on r, the separation distance between the two longitudinally separated points, of the even-order temperature structure functions is found to be reasonably well represented by the results of the analysis. The odd-order temperature structure

functions are found to deviate appreciably from their expected isotropic value. This deviation is reasonably well accounted for, at least for values of r in the inertial subrange, by a simple ramp model (Van Atta 1977) of the temperature fluctuations. The characteristic ramp appearance of the temperature signal appears to be a feature common to the temperature signal in all turbulent flows, the ramp being effectively the signature of the large-scale structure of the flow. In a boundary layer over a heated surface, the ramp structure has the form of a relatively slow increase in temperature followed by an abrupt decrease back to the level of the external stream. Temperature signals with such a ramp signature were first reported for the atmospheric boundary layer by Taylor (1958), who also observed that the arrival time of the coherent temperature structure at a fixed longitudinal position was an increasing function of height, implying a coherent structure which was tilted in the downstream direction. Kaimal & Businger (1970) identified the ramp structure in the atmospheric boundary layer with individual convecting thermal plumes being sheared by the mean velocity gradient, and Frisch & Businger (1973) inferred the statistical distribution of the plume geometry from atmospheric temperature signals. Monji (1973) found that in the atmospheric boundary layer over a salt flat the ramps could be identified at a height of only 1 cm above the ground. According to Bean *et al.* (1972) the ramp structure in some measurements over the ocean could be due to either buoyant plumes under shear or two-dimensional roll vortices. On the basis of their laboratory observations Mestayer *et al.* (1976) suggested the latter model as being generally valid for shear flows. The present ramp model assumes that the small-scale fluctuations, which are superimposed on the ramp, are isotropic and uncorrelated with the ramp statistics.

2. Experimental conditions

The temperature and velocity data were obtained on the axis of a heated round jet, with a co-flowing ambient-temperature external stream, in a laboratory thermal boundary layer and in the atmospheric surface layer over land. Measurements in the jet were made at a distance of 59 diameters downstream of the nozzle. The jet velocity was $32\,\mathrm{ms}^{-1}$ while the velocity of the zero-pressure-gradient external stream was $4{\cdot}85\,\mathrm{ms}^{-1}$.

Experimental conditions and a detailed description of the experimental technique used in the jet investigation are given in Antonia, Prabhu & Stephenson (1975). The axial (u) and radial (v) velocity fluctuations were obtained with a miniature DISA X-wire ($5\,\mu$m diameter platinum–tungsten wires) operated by two channels of DISA 55M10 constant-temperature anemometers. The temperature fluctuation was measured with a $1\,\mu$m diameter platinum 'cold' wire operated by a constant-current anemometer (the value of the current was set at $200\,\mu$A).

Measurements in the laboratory boundary layer were made well downstream of a step change in surface heat flux, with a zero external pressure gradient. The free-stream velocity was $9{\cdot}45\,\mathrm{ms}^{-1}$ and the boundary-layer thickness at the measurement station was 8·64 cm (the thermal-layer thickness was 6·0 cm). Descriptions of experimental techniques and conditions used are available in Antonia, Danh & Prabhu (1977). Velocity (streamwise u and normal v) and temperature (θ) fluctuations were obtained with an X-wire plus 'cold' wire arrangement, similar to that used for the jet.

For the atmospheric measurements, a two-wire probe was used to measure u and θ at a height of 1·4 m above the top of a wheat crop canopy at the Bungendore (New South Wales) field site of the C.S.I.R.O. Division of Environmental Mechanics. The wires were parallel and mounted in a vertical direction normal to the mean wind. The 'hot' wire (5 μm diameter platinum-coated tungsten, 1 mm long) was operated with a DISA 55M10 anemometer via a cable of length 100 m. The 1 μm diameter platinum 'cold' wire (of length 0·8 mm) was operated with a current of 200 μA and was sensitive to only temperature fluctuations. The constant-current anemometer used with this wire had a high-pass cut-off frequency at 0·02 Hz. A description of this anemometer may be found in Stellema, Antonia & Prabhu (1975).

The u and θ signals for the above three experiments were recorded on a Philips Analog 7 FM tape recorder at a speed of 38·1 cm s^{-1} (jet and boundary layer) or 9·53 cm s^{-1} (atmospheric layer). The recorded signals were later played back at a reduced speed into a sharp cut-off low-pass filter prior to digitization. The digital data were transferred to the RK 11 disc drive of the PDP 11-45 computer of the Faculty of Engineering, University of Sydney. It should be noted that the cut-off frequency f_c of the filter was set as close to the Kolmogorov frequency f_K as was conveniently possible (see table 1) while the sampling frequency was set equal to $2f_c(f_K = U/2\pi L_K)$, where U is the local velocity and L_K is the Kolmogorov length scale $\nu^{\frac{3}{4}}/\langle\epsilon\rangle^{\frac{1}{4}}$, $\langle\epsilon\rangle$ being the mean turbulent energy dissipation determined experimentally from the mean square $\langle(\partial u/\partial x)^2\rangle$ of the velocity derivative via the isotropic relation $\langle\epsilon\rangle = 15\nu\langle(\partial u/\partial x)^2\rangle$.

Using the PDP 11-45 computer, structure functions of the temperature (or velocity) were computed directly from time series of the digitized signals. The nth-order structure function of the temperature is defined as

$$\langle(\Delta\theta)^n\rangle = \langle[\theta(t+\tau)-\theta(t)]^n\rangle,$$

where τ is the time delay, which, for computational convenience, is equal to $i(2f_c)^{-1}$, where i is an integer ranging from 1 to 1000. The time structure function can be interpreted as a space structure function by using Taylor's hypothesis $r = -U\tau$, where r is now the spatial separation between the two points. As the most comprehensive sets of measurements of high-order moments of temperature structure functions have been obtained by Yeh (1971) in heated grid turbulence and Park (1976) in the boundary layer above the heated ocean, some of their measurements are compared with the present results in the following sections. Experimental conditions, including values of the local turbulence levels, are summarized in table 1.

Running moments of $\langle(\Delta\theta)^n\rangle$ and $\langle(\Delta n)^n\rangle$ for the jet flow have been calculated at intervals approximately 1 s apart. All moments, for $n = 2$–8 and for both small and large values of τ, converge to within $\pm 5\%$ of their final values after a duration of about 13 s (less than half the total record duration). A study of the convergence of the normalized structure functions $\langle(\Delta\theta)^n\rangle/\langle(\Delta\theta)^2\rangle^{\frac{1}{2}n}$ of the temperature for Park's (1976) data showed that even-order moments converge to within 5% of their final values faster than odd-order moments (this result was also noticeable in the jet data). The total times required to assure convergence to within 5% for the entire inertial subrange are about 10 min for second- and fourth-order moments, 13 min for sixth-order moments and 16 min for eighth-order moments. The corresponding times for third-, fifth- and seventh-order moments are 13 min, 20 min and 30 min, respectively. For the atmospheric data collected at Bungendore, the record length was limited to only 192 s,

Flow	R_λ	ΔT‡ (°C)	U (ms^{-1})	z (cm)	L_K (mm)	L_θ (cm)	f_K (kHz)	Sampling frequency f_s (kHz)	Duration of record (s)	$\langle u^2\rangle^{\frac{1}{2}}$ (ms^{-1})
Present										
Heated jet	188·2	3·3	7·94	—	0·12	2·45	10·5	12	21·3	0·86
Heated boundary layer	160	14	6·67	1·30	0·14	2·65	7·2	16	16	0·66
Atmospheric layer over land	1132	1·4	2·53	146	0·40	55·7	1·3	2	192	1·00
Atmospheric layer over water (Park 1976)	3200	1–2	4·95	381	0·83	—	0·93	2·085	3339	0·50
Heated grid (Yeh† 1971)	35·2	10	4·06	—	0·53	1·85	1·2	4·17	73·5	0·09

† Yeh computed the structure functions from autocorrelation functions which had been previously obtained by performing a Fourier inversion on the spectra.

‡ ΔT refers to the maximum temperature difference across the flow at the measurement station except for the atmospheric cases, where it refers to the difference between the temperature at the surface and that at the point of measurement.

TABLE 1. Summary of experimental conditions.

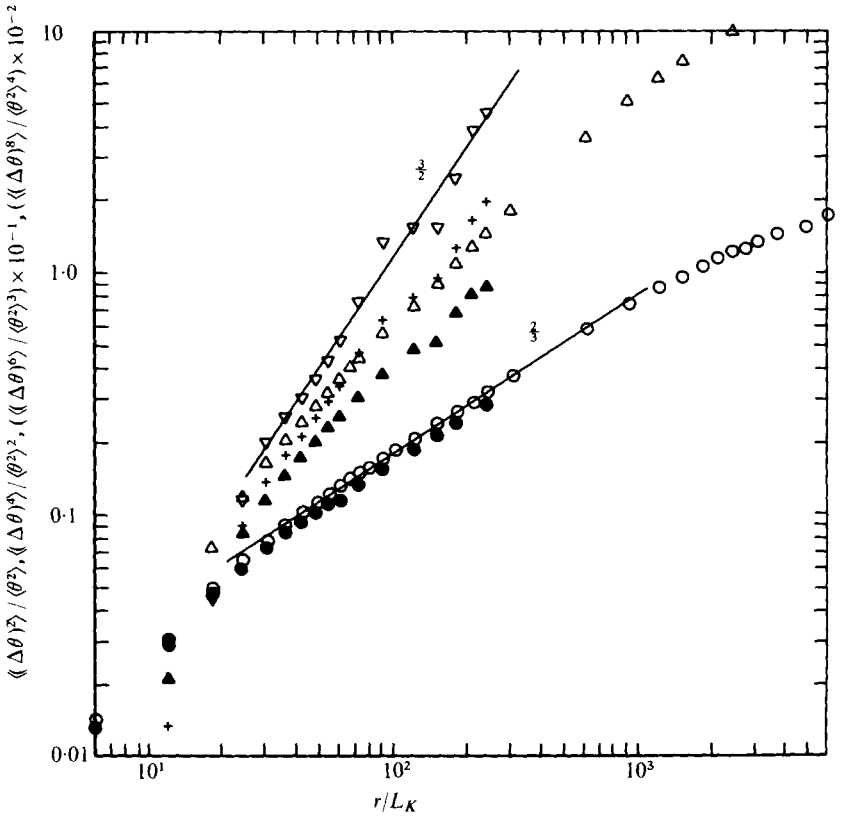

FIGURE 1 (*a*). For legend see following page.

mainly because of the relatively small available disc space on the PDP 11 computer and the relatively high frequency of 2 kHz used for sampling. From the convergence tests done on Park's data, we estimate that the accuracy for the Bungendore data is better than 20 % for both even- and odd-order moments.

3. Temperature structure functions

Normalized temperature structure functions $\langle(\Delta\theta)^n\rangle/\langle\theta^2\rangle^{\frac{1}{2}n}$ for values of n ranging from two to eight are shown as a function of r/L_K in figures 1–3, which correspond to data for the atmospheric surface layer, jet and laboratory boundary layer respectively.

The second-order structure function in the atmosphere exhibits a relatively extensive ($40 < r/L_K < 1000$) 'two-thirds' power-law dependence, which corresponds to the well-known inertial-subrange behaviour. The $r^{\frac{2}{3}}$ variation remains significant in the jet but is considerably reduced for the boundary layer, even though R_λ is approximately the same for the jet and boundary layer. The rate of increase of the higher even-order structure functions in the inertial subrange (as defined by the $\langle(\Delta\theta)^2\rangle \sim r^{\frac{2}{3}}$ dependence) becomes larger as the order increases. However, the power-law dependence seems to be retained and when n is equal to eight, the dependence is like approximately $r^{\frac{2}{3}}$ for both atmospheric and jet data. Note that the scatter exhibited by the

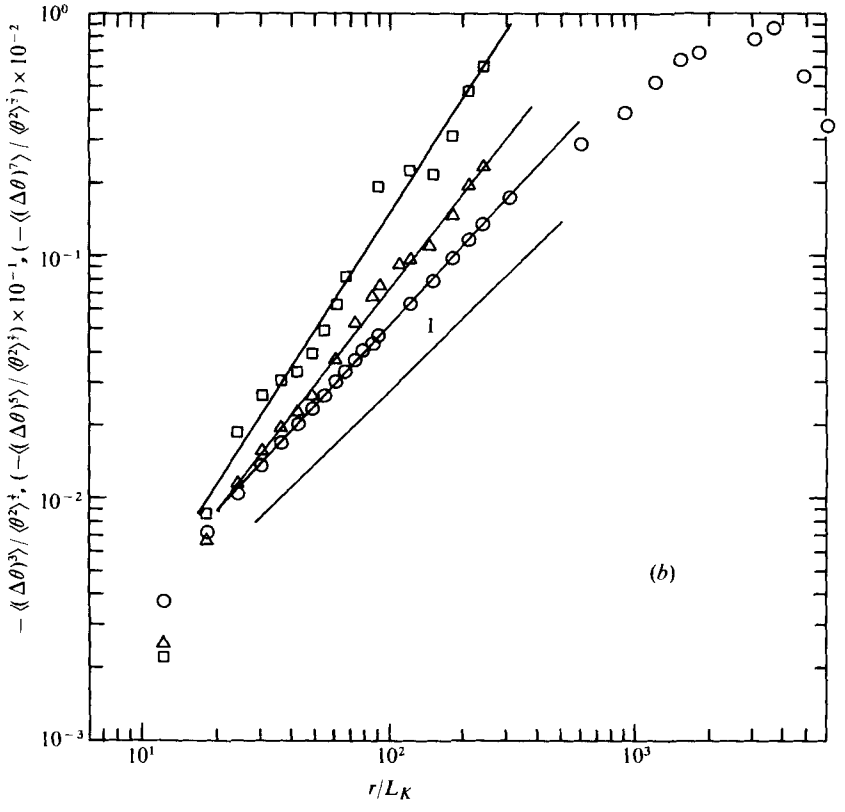

FIGURE 1. (a) Even-order temperature structure functions in atmospheric boundary layer. ○, $\langle(\Delta\theta)^2\rangle/\langle\theta^2\rangle$; △, $\langle(\Delta\theta)^4\rangle/\langle\theta^2\rangle^2$; +, $(\langle(\Delta\theta)^6\rangle/\langle\theta^2\rangle^3)\times10^{-1}$; ▽, $(\langle(\Delta\theta)^8\rangle/\langle\theta^2\rangle^4)\times10^{-2}$; ●, $\langle(\Delta\theta_T)^2\rangle/\langle\theta^2\rangle$; ▲, $\langle(\Delta\theta_T)^4\rangle/\langle\theta^2\rangle^2$. (Filled symbols denote only turbulent contributions to structure functions; cf. §4.) (b) Odd-order temperature structure functions in atmospheric boundary layer. ○, $-\langle(\Delta\theta)^3\rangle/\langle\theta^2\rangle^{\frac{3}{2}}$; △, $-(\langle(\Delta\theta)^5\rangle/\langle\theta^2\rangle^{\frac{5}{2}})\times10^{-1}$; □, $-(\langle(\Delta\theta)^7\rangle/\langle\theta^2\rangle^{\frac{7}{2}})\times10^{-2}$.

sixth-order and, in particular, the eighth-order structure functions in the atmosphere is probably due to the relatively short duration of the record used.

The main feature of the odd-order structure functions in figures 1–3 is that their magnitude departs significantly from zero, the value expected from local isotropy. This departure is also noticeable in Yeh's (1971)† measurements of $\langle(\Delta\theta)^3\rangle$ downstream of a heated grid and the published measurements of the skewness of the temperature derivative in a wide selection of turbulent shear flows.

It should be noted that the odd-order time structure functions of temperature are positive for the jet and negative in the boundary layer (both laboratory and atmospheric). This change of sign is in agreement with the reported negative and positive values for the skewness of the streamwise temperature derivative in the jet and boundary layer respectively. In the inertial subrange, the odd-order structure functions appear to exhibit a power-law dependence on τ (or r), with $\langle(\Delta\theta)^3\rangle$ increasing approxi-

† Yeh shows that a considerable part of the magnitude of the third-order structure function is due to the neglected velocity sensitivity of the cold wire. For the present measurements, the influence of the neglected velocity sensitivity on $\langle(\Delta\theta)^n\rangle$ (n odd) was found to be negligible.

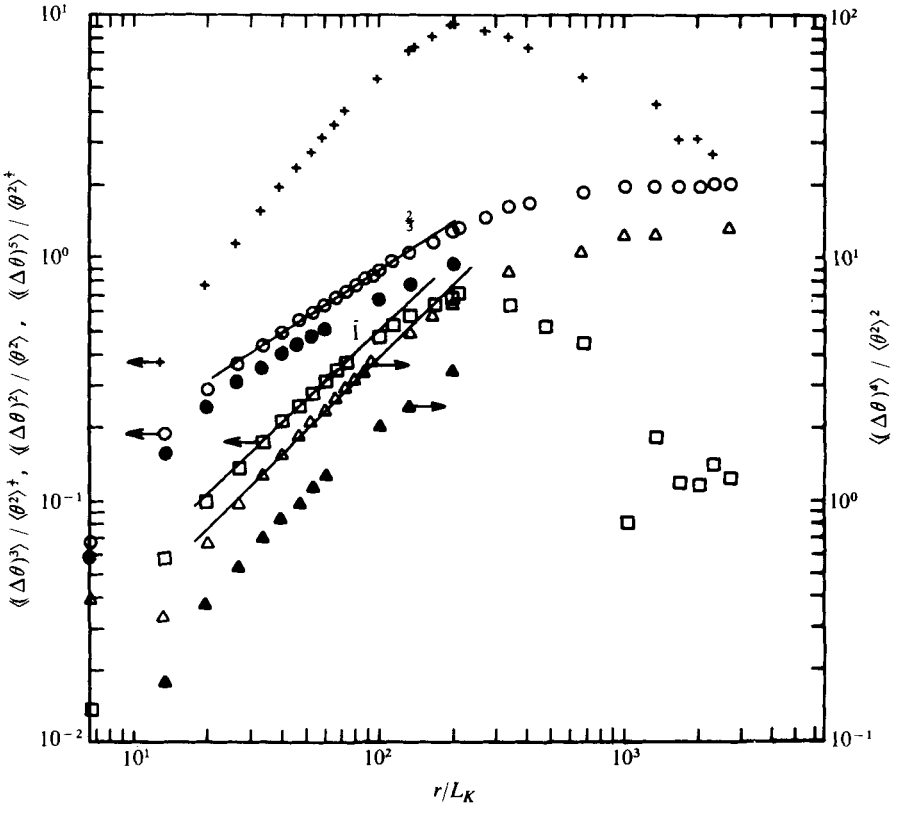

FIGURE 2(*a*). For legend see following page.

mately linearly with increasing τ in all three flows and $\langle(\Delta\theta)^5\rangle$ and $\langle(\Delta\theta)^7\rangle$ increasing at slightly faster rates. The magnitude of the odd-order functions has a maximum at relatively large values of τ in all three flows.

The time-skewness factors

$$S^n(\tau) = \langle(\Delta\theta)^n\rangle / \langle(\Delta\theta)^2\rangle^{\frac{1}{2}n} \quad (n \text{ odd})$$

and the time-flatness factors

$$F^n(\tau) = \langle(\Delta\theta)^n\rangle / \langle(\Delta\theta)^2\rangle^{\frac{1}{2}n} \quad (n \text{ even})$$

are shown in figures 4(*a*) and (*b*), respectively, for the case of the laboratory boundary layer. The skewness factors decrease significantly with increasing τ, and while they exhibit considerable scatter at large τ, they do not attain the isotropic value of zero. The magnitude of F^n (figure 4*b*) is slightly smaller than the appropriate Gaussian value at large τ.

Also shown in figure 4 are curves corresponding to various expressions derived by Frenkiel & Klebanoff (1967) which relate high-order skewness or flatness factors to lower-order ones. Frenkiel & Klebanoff assumed a Gram–Charlier probability density function to predict the departures from Gaussianity of the skewness and flatness factors of velocity structure functions in grid turbulence. It is clear from figure 4(*b*) that the

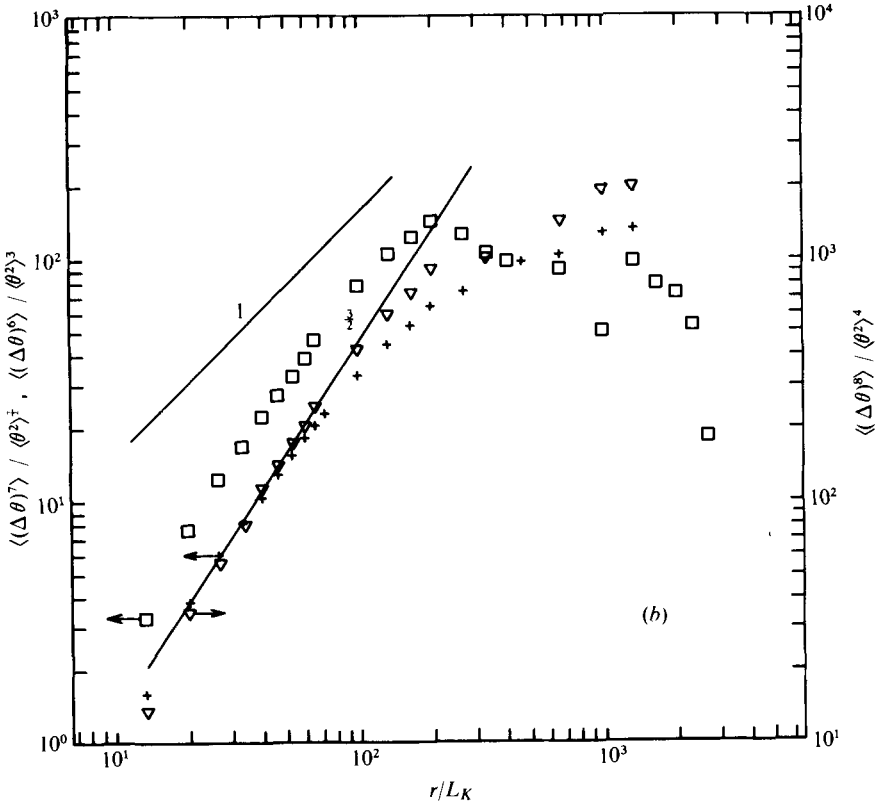

FIGURE 2. Even- and odd-order temperature structure functions in jet. (*a*) ○, $\langle(\Delta\theta)^2\rangle/\langle\theta^2\rangle$; ●, $\langle(\Delta\theta_T)^2\rangle/\langle\theta^2\rangle$; □, $\langle(\Delta\theta)^3\rangle/\langle\theta^2\rangle^{\frac{3}{2}}$; △, $\langle(\Delta\theta)^4\rangle/\langle\theta^2\rangle^2$; ▲, $\langle(\Delta\theta_T)^4\rangle/\langle\theta^2\rangle^2$; +, $\langle(\Delta\theta)^5\rangle/\langle\theta^2\rangle^{\frac{5}{2}}$. (*b*) +, $\langle(\Delta\theta)^6\rangle/\langle\theta^2\rangle^3$; □, $\langle(\Delta\theta)^7\rangle/\langle\theta^2\rangle^{\frac{7}{2}}$; ▽, $\langle(\Delta\theta)^8\rangle/\langle\theta^2\rangle^4$. (Filled symbols denote only turbulent contributions to structure functions; cf. § 4.)

sixth-order Gram–Charlier probability density is a significantly better representation of the measured hyperflatness factor F^8 than the fourth-order density. Similarly, the hyperskewness S^7 is better represented by the sixth-order ($S^7 = 21S^5 - 105S^3$) than by the fourth-order ($S^7 = 105S^3$) Gram–Charlier probability density function.

Dimensional arguments presented in Antonia & Van Atta (1975) led to an inertial-subrange behaviour of the mixed velocity–temperature structure functions given by

$$\langle(\Delta u)^m(\Delta\theta)^n\rangle = C_{mn}\, r^{\frac{1}{3}(m+n)}\langle\epsilon_r^{\frac{1}{3}m-\frac{1}{6}n}\chi_r^{\frac{1}{2}n}\rangle, \tag{1}$$

where the C_{mn} are universal constants which depend on the particular values of m and n, and where it has been assumed that the Prandtl number of the fluid is near unity. ϵ_r and χ_r represent the dissipations, averaged over a linear dimension r, of velocity and temperature fluctuations respectively. When $m = 0$,

$$\langle(\Delta\theta)^n\rangle = C_{0n}\, r^{\frac{1}{6}n}\langle\epsilon_r^{-\frac{1}{6}n}\chi_r^{\frac{1}{2}n}\rangle. \tag{2}$$

The correlation between the two dissipation fields may be written as

$$\langle\epsilon_r^{-\frac{1}{6}n}\chi_r^{\frac{1}{2}n}\rangle = \langle\epsilon\rangle^{-\frac{1}{6}n}\langle\chi\rangle^{\frac{1}{2}n}\exp(A\Omega)\,(L/r)^{\mu\Omega}, \tag{3}$$

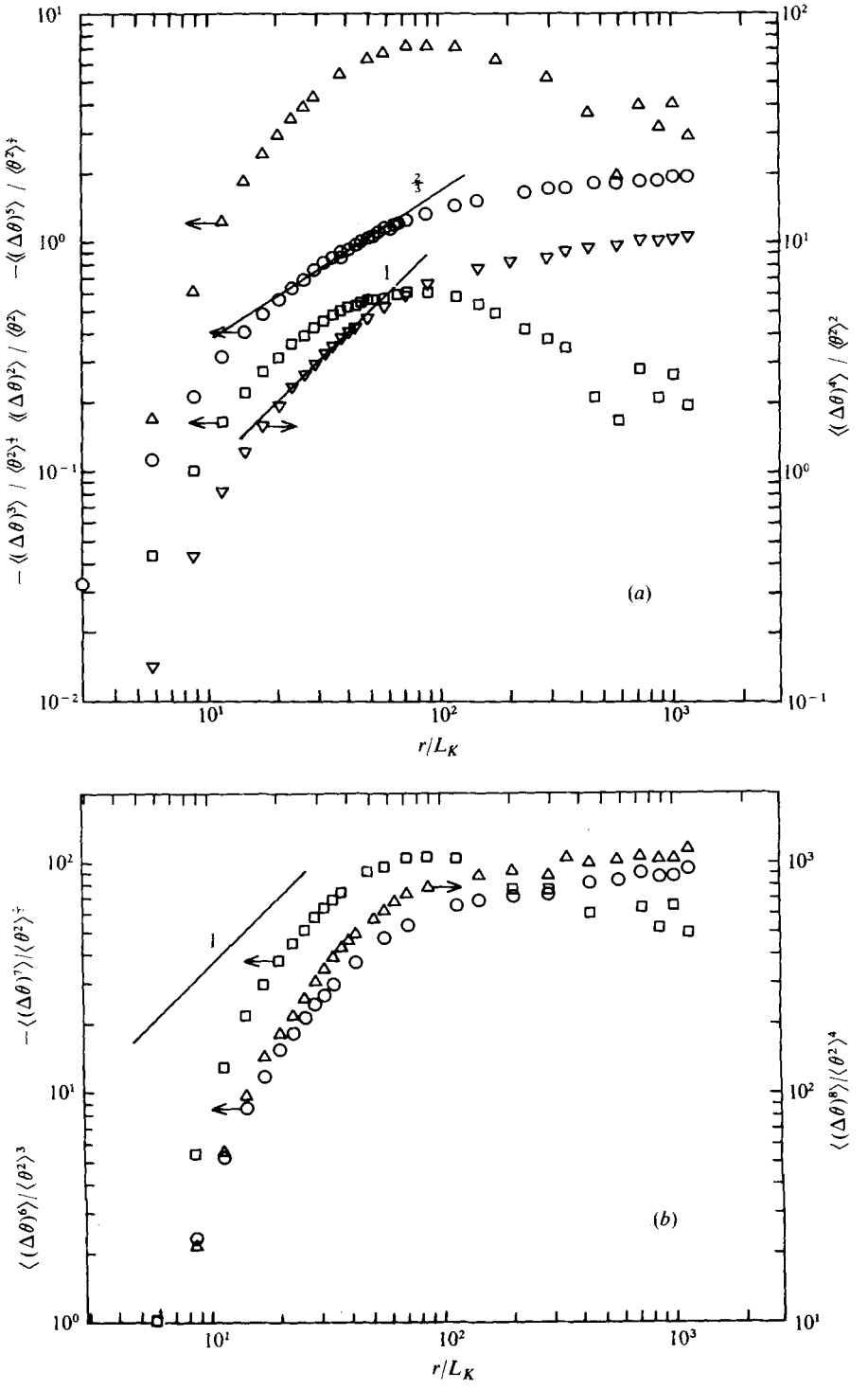

FIGURE 3. Even- and odd-order temperature structure functions in laboratory boundary layer. (*a*) ○, $\langle(\Delta\theta)^2\rangle/\langle\theta^2\rangle$; □, $-\langle(\Delta\theta)^3\rangle/\langle\theta^2\rangle^{\frac{3}{2}}$; ▽, $\langle(\Delta\theta)^4\rangle/\langle\theta^2\rangle^2$; △, $-\langle(\Delta\theta)^5\rangle/\langle\theta^2\rangle^{\frac{5}{2}}$. (*b*) ○, $\langle(\Delta\theta)^6\rangle/\langle\theta^2\rangle^3$; □, $-\langle(\Delta\theta)^7\rangle/\langle\theta^2\rangle^{\frac{7}{2}}$; △, $\langle(\Delta\theta)^8\rangle/\langle\theta^2\rangle^4$.

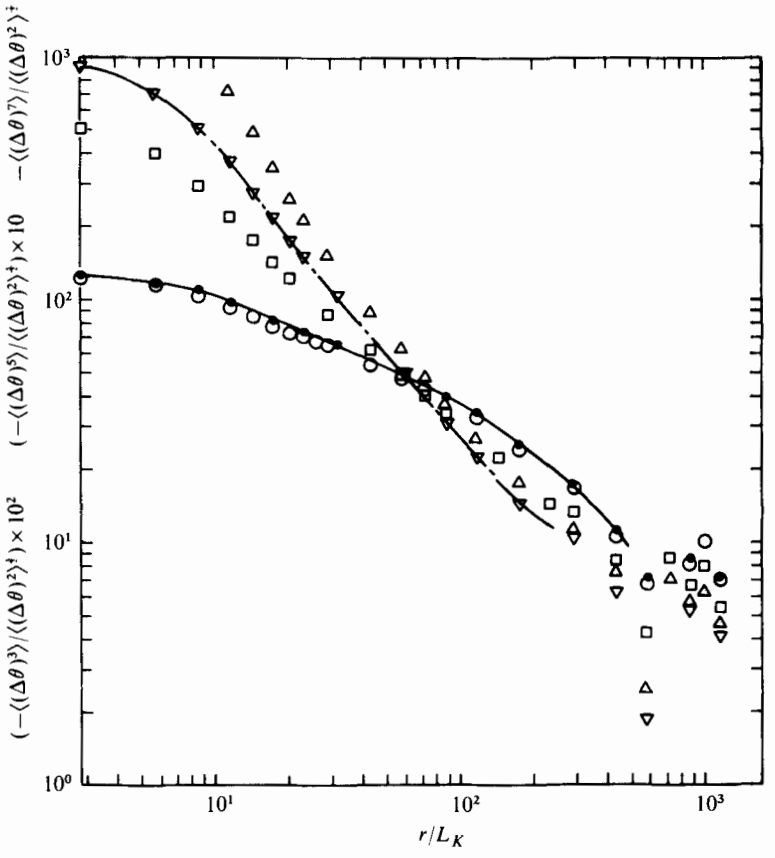

FIGURE 4(a). For legend see facing page.

where $\Omega = \frac{1}{12}n(\frac{5}{3}n - n\rho - 2)$, $\rho(r)$ is the correlation coefficient between $\ln\chi_r$ and $\ln\epsilon_r$, and the following assumptions have been made:

(i) that ϵ_r and χ_r are lognormally distributed and their joint probability density is bivariate lognormal;

(ii) that the variances of $\ln\epsilon_r$ and $\ln\chi_r$ are both given by (Kolmogorov 1962; Oboukhov 1962; see also Antonia & Van Atta 1975)

$$\sigma^2 = A + \mu\ln(L/r), \tag{4}$$

where A is a universal constant and L is the turbulence length scale.

Expression (2) can now be written as

$$\langle(\Delta\theta)^n\rangle = C_{0n}r^{\frac{1}{3}n}\langle\chi\rangle^{\frac{1}{2}n}\langle\epsilon\rangle^{-\frac{1}{6}n}\exp(A\Omega)(L/r)^{\mu\Omega}. \tag{5}$$

With $\mu = \frac{1}{2}$ and $\rho = \frac{2}{3}$, the values used by Antonia & Van Atta (1975), the inertial-subrange variations of $\langle(\Delta\theta)^2\rangle$, $\langle(\Delta\theta)^4\rangle$, $\langle(\Delta\theta)^6\rangle$ and $\langle(\Delta\theta)^8\rangle$ are given by $r^{\frac{2}{3}}$, r, r and $r^{\frac{2}{3}}$ respectively. The original two-thirds variation for the second-order structure function is unchanged but the modified analysis predicts variations of higher even-order moments which are in closer agreement with the data than the predictions of the original theory. When $n = 8$, the previously mentioned experimental variation is like $r^{\frac{8}{3}}$ while the modified and original analyses yield $r^{\frac{8}{3}}$ and $r^{\frac{8}{3}}$ variations respectively. As

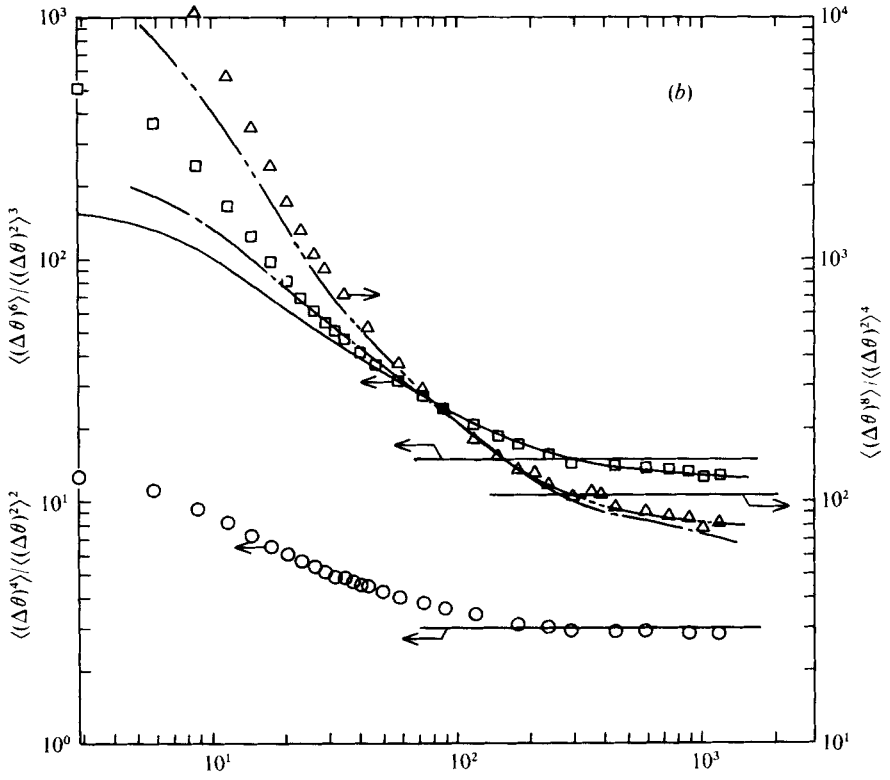

FIGURE 4. (*a*) Skewness factors of structure functions in laboratory boundary layer. ○, $-S^3 \times 10^2$; □, $-S^5 \times 10$; △, $-S^7$; —●—, $S^7 = 105S^3$; -▽—·—, $S^7 = 21S^5 - 105S^3$. (*b*) Flatness factors of structure functions in laboratory boundary layer. ○, F^4; □, F^6; △, F^8; ——, $F^6 = 15F^4 - 30$; —·—, $F^8 = 210F^4 - 525$; —··—, $F^8 = 28F^6 - 210F^4 + 315$. Horizontal lines refer to Gaussian values ($F^4 = 3$, $F^6 = 15$, $F^8 = 105$).

found by Van Atta & Park (1972), the modified Kolmogorov analysis consistently underestimated the observed power of r, while the original (1941) theory overestimated it.†

The flatness factors of $\Delta\theta$ for the jet and the high R_λ data, plotted in figure 5 as a function of r/L_K, show a $-\frac{1}{3}$ dependence in the inertial subrange, in agreement with the prediction of the modified theory. The slope of the superflatness factors in the inertial subrange, shown in figure 6, is not quite as steep as r^{-1}, but it is closer to the prediction of the modified theory than to that of Kolmogorov's 1941 theory. At small values of r,

$$\langle(\Delta\theta)^n\rangle/\langle(\Delta\theta)^2\rangle^{\frac{1}{2}n} \to \langle(\partial\theta/\partial x)^n\rangle/\langle(\partial\theta/\partial x)^2\rangle^{\frac{1}{2}n},$$

so that the flatness factor of $\Delta\theta$ should approach the value of the flatness factor of the temperature derivative. The measured flatness factor of the derivative is indicated in figure 5. Figures 5 and 6 show that the present atmospheric data are in close agreement with Park's (1976) data and reveal that Mestayer's (1975) data obtained in the Marseille wind–water tunnel at a relatively large laboratory R_λ lie between the present

† Note, however, that the exponent of r in the modified analysis is zero for $n = 10$ and negative at larger n, whereas the experimental values continue to increase positively.

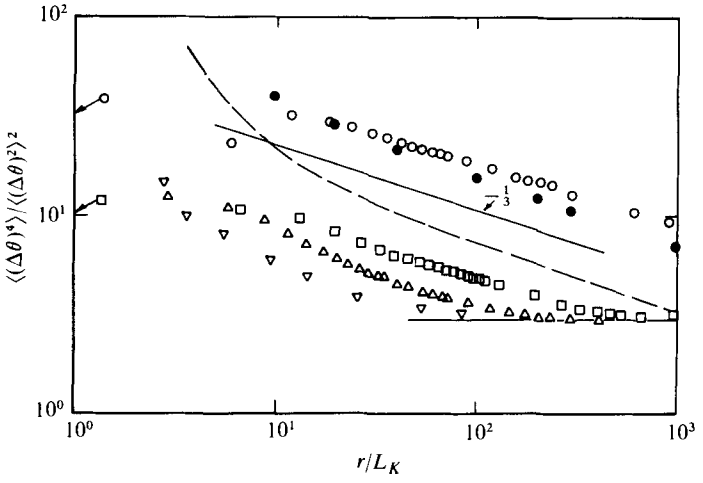

FIGURE 5. Reynolds number dependence of flatness factor of temperature structure function. ∇, grid turbulence (Yeh 1971), $R_\lambda = 35{\cdot}2$; $\triangle$, laboratory boundary layer, $R_\lambda = 160$; $\square$, jet, $R_\lambda = 188{\cdot}2$; $\bigcirc$, atmospheric boundary layer over land, $R_\lambda = 1132$; $\bullet$, atmospheric boundary layer over water (Park 1976), $R_\lambda = 3200$; ———, laboratory boundary layer (Mestayer 1975), $R_\lambda = 1050$. Horizontal line refers to Gaussian value ($F^4 = 3$). Arrows indicate values of flatness factors of the temperature derivative.

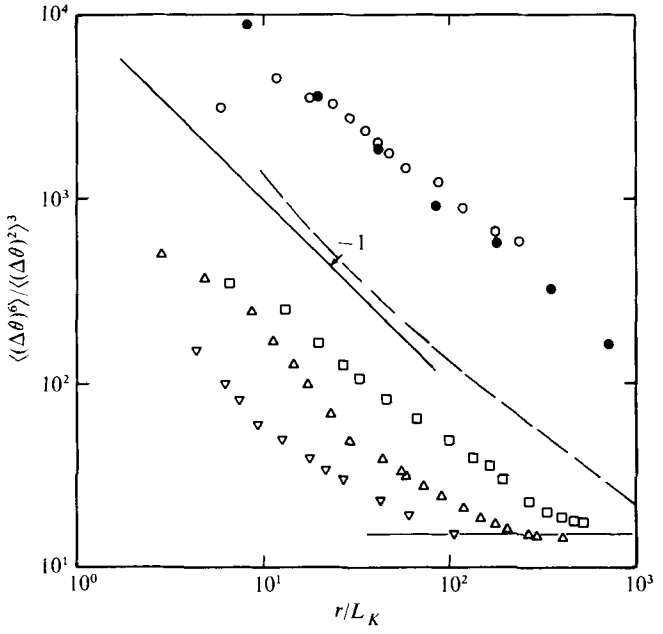

FIGURE 6. Reynolds number dependence of superflatness factor of temperature structure function. Symbols are as in figure 5. Horizontal line refers to Gaussian value ($F^6 = 15$).

laboratory data and the atmospheric data. The significant dependence on R_λ of the flatness and superflatness factors of $\Delta\theta$ is clearly demonstrated in figures 5 and 6. The predicted Reynolds number dependence of the modified analysis can be inferred from (5), since

$$\langle(\Delta\theta)^n\rangle/\langle(\Delta\theta)^2\rangle^{\frac{1}{2}n} \sim (L/r)^{\mu(\Omega-\frac{1}{2}n\Omega')}, \tag{6}$$

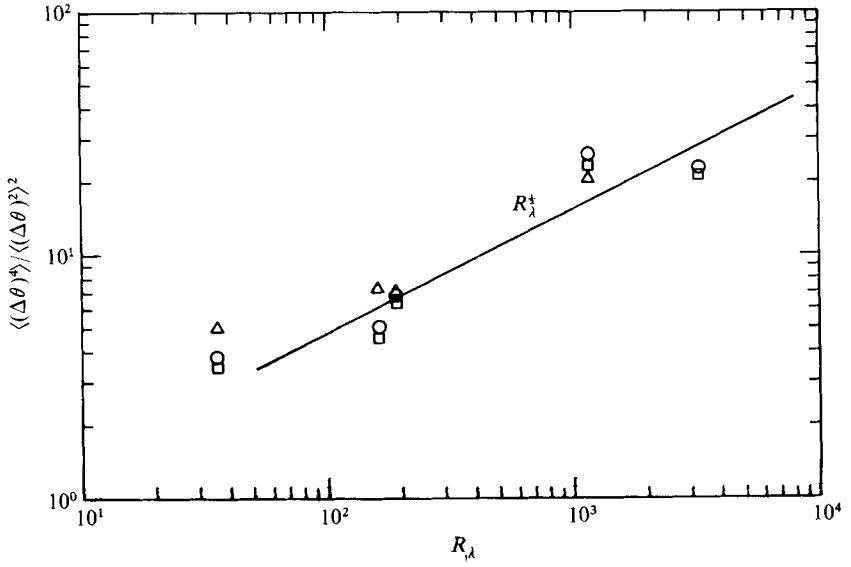

FIGURE 7. Reynolds number dependence of F^4 for fixed values of r/L_K. ○, $r/L_K = 30$; □, $r/L_K = 40$; △, $r = \lambda$.

where $\Omega' = \frac{1}{3}(\frac{2}{3} - \rho)$.

For a given value of r/L_K, (6) can be written as

$$\langle(\Delta\theta)^n\rangle/\langle(\Delta\theta)^2\rangle^{\frac{1}{2}n} \sim R_\lambda^{\frac{3}{2}\mu(\Omega - \frac{1}{2}n\Omega')} \tag{7}$$

since $L/L_K \sim R_\lambda^{\frac{3}{2}}$ for isotropic turbulence. When $\rho = \frac{2}{3}$, $\Omega' = 0$ and $\Omega = \frac{2}{3}$, so that

$$F^4 \sim R_\lambda^\mu. \tag{8}$$

With $\mu = \frac{1}{2}$, F^4 varies as $R_\lambda^{\frac{1}{2}}$, as indicated in figure 7 together with the present experimental values of F^4 and those of Yeh (1971) and Park (1976) for values of r of $30L_K$ and $40L_K$ respectively. The increase in F^4 with R_λ is supported qualitatively by the data, but in view of the large scatter in the data and the relatively small R_λ range for which atmospheric data are available, it is difficult to make a meaningful comparison with (8).†

The third-order correlation $\langle(\Delta u)(\Delta\theta)^2\rangle$ and the fourth-order correlation $\langle(\Delta u)^2(\Delta\theta)^2\rangle$ are shown in figures 8 and 9 for the atmospheric and jet data respectively. The variation with r of $\langle(\Delta u)(\Delta\theta)^2\rangle$ is approximately linear over the inertial subrange, in agreement with Yaglom's (1949) result

$$\langle(\Delta u)(\Delta\theta)^2\rangle = -\tfrac{4}{3}\langle\chi\rangle r, \tag{9}$$

derived from consideration of the scalar conservation equation for a homogeneous and isotropic field of turbulence. Figure 10, which uses co-ordinates normalized by Kolmogorov velocity (u_K), time (τ_K) and length (L_K) scales, shows that (9) is in close agree-

† Also shown in figure 7 are the experimental values of F^4 obtained by setting r equal to λ, the easily measured Taylor microscale. When $r = \lambda$, (6) yields $F^n \sim R_\lambda^{\mu\Omega}$ as $L/\lambda \sim R_\lambda$ in isotropic turbulence. For $\mu = \frac{1}{2}$, $F^4 \sim R_\lambda^{\frac{1}{2}}$. This reduced rate of increase of F^4 seems to be qualitatively supported by the data in figure 7.

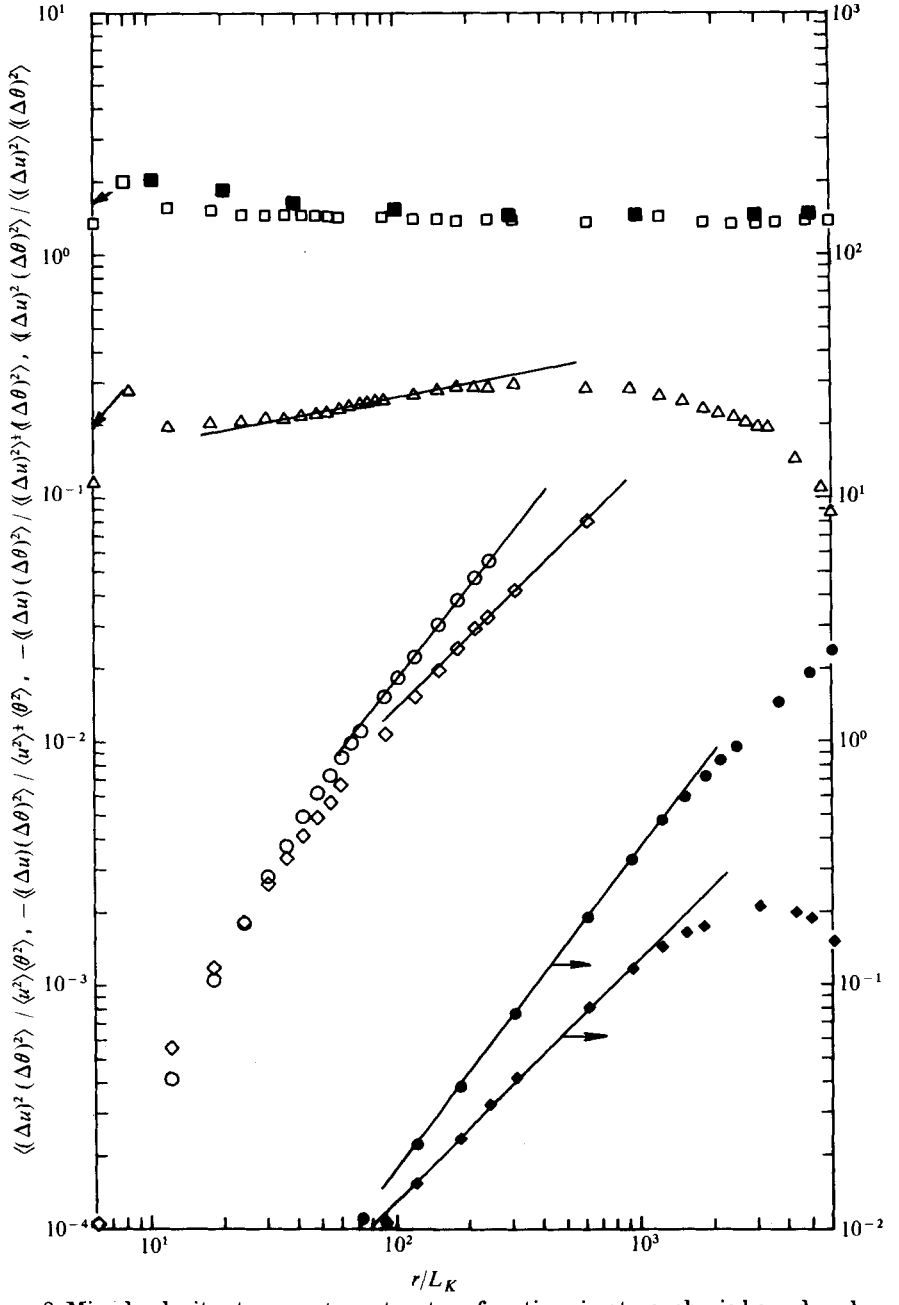

FIGURE 8. Mixed velocity–temperature structure functions in atmospheric boundary layer. ◇, ◆, $-\langle(\Delta u)(\Delta\theta)^2\rangle/\langle u^2\rangle^{\frac{1}{2}}\langle\theta^2\rangle$; ○, ●, $\langle(\Delta u)^2(\Delta\theta)^2\rangle/\langle u^2\rangle\langle\theta^2\rangle$; △, $-\langle(\Delta u)(\Delta\theta)^2\rangle/\langle(\Delta u)^2\rangle^{\frac{1}{2}}\langle(\Delta\theta)^2\rangle$; □, $\langle(\Delta u)^2(\Delta\theta)^2\rangle/\langle(\Delta u)^2\rangle\langle(\Delta\theta)^2\rangle$; ■, $\langle(\Delta u)^2(\Delta\theta)^2\rangle/\langle(\Delta u)^2\rangle\langle(\Delta\theta)^2\rangle$, Park (1976).

ment with both jet and atmospheric data.† While the mixed velocity–temperature skewness $\langle(\Delta u)(\Delta\theta)^2\rangle/\langle(\Delta u)^2\rangle^{\frac{1}{2}}\langle(\Delta\theta)^2\rangle$ is nearly constant over the inertial subrange, the ratio $\langle(\Delta u)^2(\Delta\theta)^2\rangle/\langle(\Delta u)^2\rangle\langle(\Delta\theta)^2\rangle$ is remarkably constant over almost the complete range of r under investigation. The values of these two constants are only slightly

† For the experimental data, the isotropic value of $\langle\chi\rangle = 3\alpha\langle(\partial\theta/\partial x)^2\rangle$ has been used.

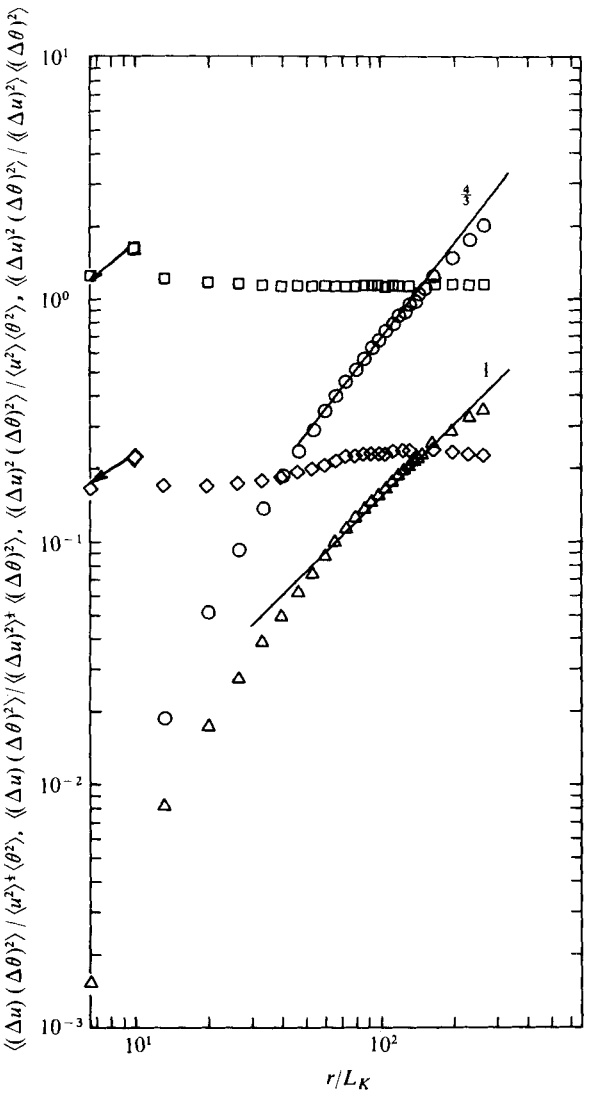

FIGURE 9. Mixed velocity–temperature structure functions in the jet. △, $\langle(\Delta u)(\Delta\theta)^2\rangle/\langle u^2\rangle^{\frac{1}{2}}\langle\theta^2\rangle$; ◇, $\langle(\Delta u)(\Delta\theta)^2\rangle/\langle(\Delta u)^2\rangle^{\frac{1}{2}}\langle(\Delta\theta)^2\rangle$; ○, $\langle(\Delta u)^2(\Delta\theta)^2\rangle/\langle u^2\rangle\langle\theta^2\rangle$; □, $\langle(\Delta u)^2(\Delta\theta)^2\rangle/\langle(\Delta u)^2\rangle\langle(\Delta\theta)^2\rangle$.

larger for the atmospheric than for the jet data. In the analysis of Antonia & Van Atta (1975), it was shown that for the lognormal model

$$\frac{\langle(\Delta u)(\Delta\theta)^2\rangle}{\langle(\Delta u)^2\rangle^{\frac{1}{2}}\langle(\Delta\theta)^2\rangle} = \frac{C_{12}}{C_{20}^{\frac{1}{2}}C_{02}}\exp\left[\frac{A}{3}(\rho-\tfrac{1}{2})\right]\left(\frac{L}{r}\right)^{\frac{1}{3}\mu(\rho-\frac{1}{2})} \tag{10}$$

and

$$\frac{\langle(\Delta u)^2(\Delta\theta)^2\rangle}{\langle(\Delta u)^2\rangle\langle(\Delta\theta)^2\rangle} = \frac{C_{22}}{C_{20}C_{02}}\exp\left[\tfrac{2}{3}A(\rho-\tfrac{2}{3})\right]\left(\frac{L}{r}\right)^{\frac{2}{3}\mu(\rho-\frac{1}{2})}. \tag{11}$$

From the atmospheric data of Paquin & Pond (1971), appropriate values for C_{20} and C_{02} are 2 and 1·6 respectively. With the assumption that C_{12} is equal to $-\frac{2}{3}$ [equation (9)], the coefficient $C_{12}/(C_{20}^{\frac{1}{2}}C_{02})$ in (10) is $-0{\cdot}29$. This number is in excellent

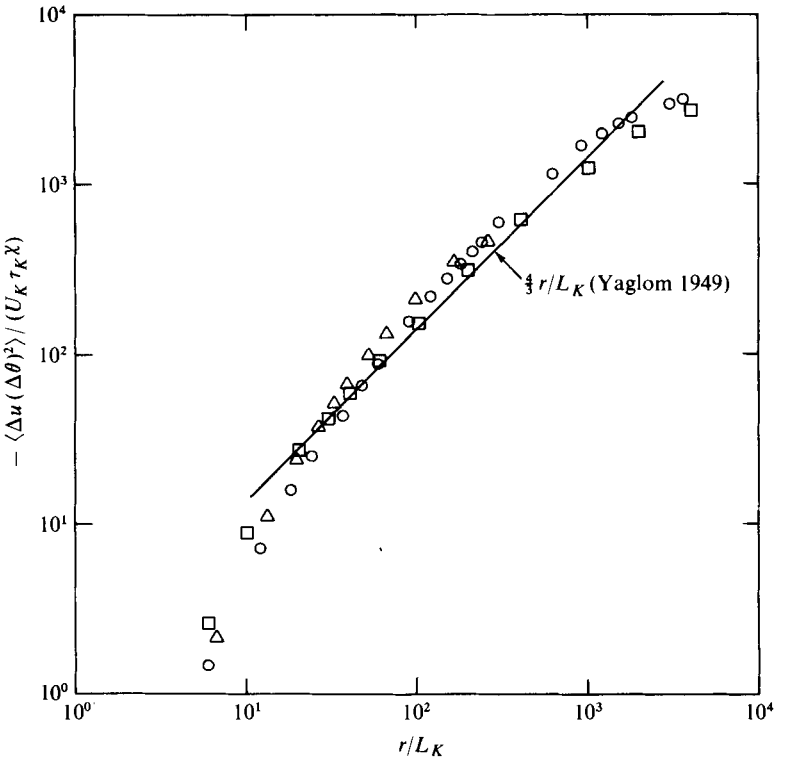

FIGURE 10. Mixed velocity–temperature structure functions normalized by Kolmogorov scales. △, jet; ○, atmospheric boundary layer over land; □, atmospheric boundary layer over ocean (Park 1976).

agreement with that obtained from atmospheric data in the inertial subrange by Paquin & Pond (1971) and Gurvich & Zubkovskii (1966). The present atmospheric data (figure 8) indicate a value of $-0{\cdot}28$ while the jet data (figure 9) yield a slightly larger value of $-0{\cdot}24$. For the low R_λ data of Yeh, $\langle(\Delta u)\,(\Delta\theta)^2\rangle/\langle(\Delta u)^2\rangle^{\frac{1}{2}}\langle(\Delta\theta)^2\rangle$ was found to be in the range $-0{\cdot}30$ to $0{\cdot}22$† when r/L_K is in the range $15L_K$ to $30L_K$. The results of figure 8 suggest that $C_{22}/C_{20}C_{02}$ is approximately equal to 1·4, so that $C_{22} \simeq 4{\cdot}5$.‡

As τ (or r) approaches zero, the ratios on the left-hand sides of (10) and (11) should tend to S_T ($\equiv \langle(\partial u/\partial x)\,(\partial\theta/\partial x)^2\rangle/\langle(\partial u/\partial x)^2\rangle^{\frac{1}{2}}\langle(\partial\theta/\partial x)^2\rangle$) and

$$\langle(\partial u/\partial x)^2\,(\partial\theta/\partial x)^2\rangle/\langle(\partial u/\partial x)^2\rangle\langle(\partial\theta/\partial x)^2\rangle$$

respectively. This is indeed found to be the case in figures 8 and 9. The slight increase in S_T from the jet (figure 8) to the atmospheric data (figure 9) is in qualitative agreement with the R_λ trend of S_T predicted by Van Atta (1974).

† These values were obtained from the measured second- and third-order time correlation coefficients since

$$\langle(\Delta u)\,(\Delta\theta)^2\rangle/\langle u^2\rangle^{\frac{1}{2}}\langle\theta^2\rangle = R_{\theta^2,u} - 2R_{\theta,u\theta} + 2R_{u\theta,\theta} - R_{u,\theta^2} \quad \text{and} \quad \langle(\Delta u)^2\rangle/\langle u^2\rangle = 2(1-R_{u,u}),$$

where the R's are correlation coefficients normalized by appropriate powers of $\langle u^2\rangle$ and $\langle\theta^2\rangle$.

‡ The values of C_{12} and C_{22} are not likely to be seriously affected by the actual value of ρ. Note that $\rho = \frac{2}{3}$ was obtained from low R_λ jet data.

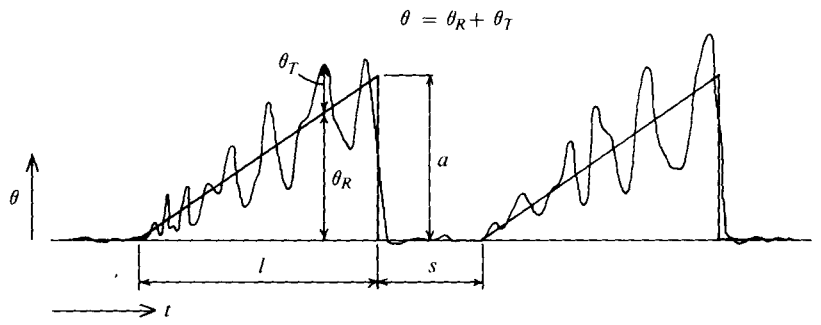

FIGURE 11. Ramp model of temperature.

4. Effect of temperature ramps on structure functions

The behaviour of odd-order structure functions of θ presented in the previous section is in obvious disagreement with predictions of high Reynolds number local similarity theory. Van Atta (1977) has already noted that this behaviour appears to be a consequence of the presence of a large-scale coherent temperature structure in the atmospheric temperature signal. The signature of this large-scale structure in the temperature is not confined to the atmospheric situation as it has also been observed in various turbulent flows in the laboratory. The simplest model that has been used to represent the effect of this large-scale structure is sketched in figure 11. In this sketch, θ is simply assumed to be made up of the linear superposition of θ_R, a linear ramp, and θ_T, which represents 'turbulent' fluctuations whose characteristic time (or length) scale is significantly smaller than that of θ_R. The ramp is characterized by a slow linear increase with time followed by an abrupt sharp decrease.† With the assumption that $(\Delta\theta)_T$ and $(\Delta\theta)_R$ are statistically independent, Van Atta (1977) obtains

$$\langle(\Delta\theta)^3\rangle = \langle(\Delta\theta_T)^3\rangle + \langle(\Delta\theta_R)^3\rangle \tag{12}$$

and shows that a good approximation to $\langle(\Delta\theta_R)^n\rangle$ in the inertial–convective subrange is given by

$$\langle(\Delta\theta_R)^n\rangle = (\pm 1)^n a^n r/(l+s) \tag{13}$$

(plus sign for jet, minus sign for boundary layer) to first order in r (it is assumed that our interest lies mainly in inertial-range values of r which are small compared with $l+s$). In this expression, a is the amplitude of the ramp (figure 11), l is the length of the ramp and s is the length of the quiescent period between consecutive ramps. With the further assumption that the small-scale properties of θ_T are locally isotropic, so that $\langle(\Delta\theta_T)^n\rangle = 0$, when n is odd, an equation for the ramp amplitude can be found:

$$a^3 + [10\langle(\Delta\theta)^2\rangle - \langle(\Delta\theta)^5\rangle/\langle(\Delta\theta)^3\rangle]\,a \pm 10\langle(\Delta\theta)^3\rangle = 0 \tag{14}$$

(plus sign for boundary layer, minus sign for jet), so that a can be estimated from the measured values of second-, third- and fifth-order structure functions of $\Delta\theta$. Values of $a/\langle\theta^2\rangle^{\frac{1}{2}}$ are shown in figure 12 and are approximately constant over a significant range of r/L_K. Values of $l+s$, the distance between consecutive ramps, obtained using (12) and (13), are given by

$$l+s = \pm a^3 r/\langle(\Delta\theta)^3\rangle \tag{15}$$

† Note that the direction of this ramp is the same in the laboratory boundary layer. In the jet, the ramp is reversed in time.

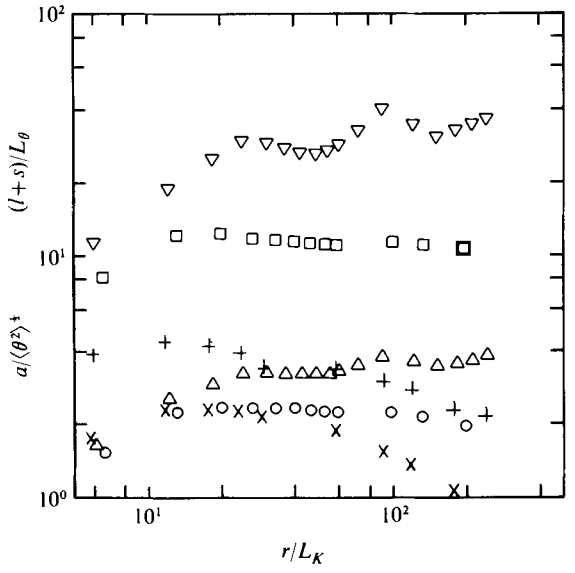

FIGURE 12. Height and length of ramps for laboratory and atmospheric data. Jet: ○, $a/\langle\theta^2\rangle^{\frac{1}{2}}$; □, $(l+s)/L_\theta$. Laboratory boundary layer: ×, $a/\langle\theta^2\rangle^{\frac{1}{2}}$; +, $(l+s)/L_\theta$. Atmospheric boundary layer over land: △, $a/\langle\theta^2\rangle^{\frac{1}{2}}$; ▽, $(l+s)/L_\theta$.

(minus sign for boundary layer, plus sign for jet). As shown in figure 12, the values of $l+s$ are remarkably constant in the case of the jet, being equal to approximately $11L_\theta$, where L_θ is an integral length scale† of the turbulence. The ratio $(l+s)/L_\theta$ is not nearly as constant for the atmospheric data, but its magnitude emphasizes the relatively large scale of the atmospheric ramps in comparison with the turbulence length scale and the inertial-range scales of r. The frequency of occurrence of the atmospheric ramps is $U/(l+s) \simeq 8\,\mathrm{min}^{-1}$, which is in reasonable agreement with the frequency of 5–7 min^{-1} obtained by Van Atta from Park's atmospheric data and significantly smaller than the repetition rate of 30 s^{-1} for the jet ramps. It should be noted that the values of $a/\langle\theta^2\rangle^{\frac{1}{2}}$ and $(l+s)/L_\theta$ for the jet ramps are in good agreement with mean values for these two quantities inferred from temperature traces displayed on an ultra-violet strip-chart recorder. A linear ramp model similar to that shown in figure 11 was used by Antonia & Atkinson (1976) to explain some of the measured high-order moments of temperature in the jet. A more elaborate model was also developed for the ramp structure with an exponential, instead of linear, mean ramp distribution and with allowance for the random length of the ramp. It is possible that this more realistic model of the ramp may be used to explain the behaviour of the moments of the temperature structure function of higher (even and odd) order. The extra complications do not seem warranted at present in view of the reasonable success of the linear ramp model in predicting the main features of the anisotropy of the large-scale temperature structure.

Using the computed values of a, the contributions $\langle(\Delta\theta_T)^2\rangle$ and $\langle(\Delta\theta_T)^4\rangle$ of the turbulent fluctuations to the second- and fourth-order temperature structure functions are indicated in figures 1(a) and 2(a). The contribution $\langle(\Delta\theta_T)^2\rangle$ ($= \langle(\Delta\theta)^2\rangle + \langle(\Delta\theta)^3\rangle/a$)

† Determined from the area under the temperature autocorrelation curve.

is very nearly equal to $\langle(\Delta\theta)^2\rangle$, especially in the case of the atmospheric data, which suggests that the contribution from the ramp to $\langle(\Delta\theta)^2\rangle$ is almost negligible. The contribution from $\langle(\Delta\theta_T)^4\rangle$ represents 60–70 % of $\langle(\Delta\theta)^4\rangle$ over the inertial subrange of the atmospheric data. The rate of increase of $\langle(\Delta\theta_T)^4\rangle$ with r in the inertial subrange is slightly slower than that for $\langle(\Delta\theta)^4\rangle$. This trend is encouraging as it suggests even closer agreement between the measurements and the predictions of the modified theory. It must be noted, however, that the measured fifth- and seventh-order moments of $\Delta\theta$ increase at a somewhat faster rate than the linear rate indicated by (13). With regard to mixed velocity–temperature structure functions, Van Atta (1976) showed that for the present model the correlation $\langle(\Delta u)(\Delta\theta)^2\rangle$ is unaffected by the ramps,

viz. $$\langle(\Delta u)(\Delta\theta)^2\rangle = \langle(\Delta u_T)(\Delta\theta_T)^2\rangle,$$

provided that Δu is statistically independent of $\Delta\theta_R$ and $\Delta\theta_T$. Examination of the present simultaneous records of u and θ lends some support to the last assumption as there is no strong evidence of a ramp structure for u, even though good correlation exists between low frequency components of u and θ.

5. Concluding remarks

The behaviour of the odd-order structure functions of the temperature measured in different flows is in basic disagreement with predictions of high Reynolds number local similarity theory. This disagreement appears to be a direct result of the observed anisotropic coherent large-scale features of shear-flow turbulence. A simple ramp model for the large-scale structure correctly predicts the sign of the odd-order structure functions and yields a good approximation to their variation with r. A closer prediction of the variation with r of the higher odd-order moments of $\Delta\theta$ probably requires a less idealized model for the ramps. An exponential model for the ramps was used by Antonia & Atkinson (1976) to calculate the high-order moments of θ. However, the implementation of such a model for the atmospheric data does not, at present, appear to be straightforward. It would appear that a quantitative model which adequately explains the observed non-zero skewness of the temperature derivative is not yet within easy reach.

The removal of the effects of the coherent structure using the present ramp model does not radically change the slope of even-order temperature structure functions. The analysis presented in Antonia & Van Atta (1975) is in much closer agreement with the measured slope than the original Kolmogorov theory. It is hoped that an improved ramp model may explain the discrepancy that at present exists between the predictions of the analysis and the measured higher even-order moments of $\Delta\theta$.

One of the authors (R. A. A.) is grateful to Dr E. F. Bradley (C.S.I.R.O. Department of Environmental Mechanics) for the use of facilities at the Bungendore field site. He also acknowledges the support of the Australian Research Grants Committee. At San Diego, C.W.V.A.'s work was supported by N.S.F. Grant ENG76-13147 and by the Office of Naval Research under Grant NR 062-544.

REFERENCES

ANTONIA, R. A. & ATKINSON, J. D. 1976 A ramp model for turbulent temperature fluctuations. *Phys. Fluids* **19**, 1273.

ANTONIA, R. A., DANH, H. Q. & PRABHU, A. 1977 Response of a turbulent boundary layer to a step change in surface heat flux. *J. Fluid Mech.* **80**, 153.

ANTONIA, R. A., PRABHU, A. & STEPHENSON, S. E. 1975 Conditionally sampled measurements in a heated turbulent jet. *J. Fluid Mech.* **72**, 455.

ANTONIA, R. A. & VAN ATTA, C. W. 1975 On the correlation between temperature and velocity dissipation fields in a heated turbulent jet. *J. Fluid Mech.* **67**, 273.

BEAN, B. R., GILMER, R., GROSSMANN, R. L. & MCGAVIN, R. 1972 An analysis of airborne measurements of vertical water vapor during BOMEX. *J. Atmos. Sci.* **29**, 860.

FRENKIEL, F. N. & KLEBANOFF, P. S. 1967 Higher-order correlations in a turbulent field. *Phys. Fluids* **10**, 507.

FRISCH, A. S. & BUSINGER, J. A. 1973 A study of convective elements in the atmospheric surface layer. *Boundary-Layer Met.* **3**, 301.

GURVICH, A. S. & ZUBKOVSKII, S. L. 1966 Evaluation of structural characteristics of temperature pulses in the atmosphere. *Izv. Atmos. Ocean. Phys.* **2**, 202.

KAIMAL, J. C. & BUSINGER, J. A. 1970 Case studies of a convective plume and a dust devil. *J. Appl. Met.* **9**, 612.

KOLMOGOROV, A. N. 1941 The local structure of turbulence in incompressible viscous fluid for very large Reynolds numbers. *C. R. Acad. Sci. USSR* **30**, 301–305.

KOLMOGOROV, A. N. 1962 A refinement of previous hypotheses concerning the local structure of turbulence in a viscous incompressible fluid at high Reynolds number. *J. Fluid Mech.* **13**, 82.

MESTAYER, P. G. 1975 Étude de certaines caractéristiques statistiques locales d'une couche limite turbulente à grand nombre de Reynolds. Thèse Docteur–Ingénieur, Université d'Aix–Marseille, France.

MESTAYER, P. G., GIBSON, C. H., COANTIC, M. F. & PATEL, A. S. 1976 Local isotropy in heated and cooled turbulent boundary layers. *Phys. Fluids* **19**, 1279.

MONJI, N. 1973 Budgets of turbulent energy and temperature variance in the transition zone from forced to free convection. *J. Met. Soc. Japan* **51**, 133.

OBOUKHOV, A. M. 1962 Some specific features of atmospheric turbulence. *J. Fluid Mech.* **13**, 77.

PAQUIN, J. E. & POND, S. 1971 The determination of the Kolmogorov constants for velocity, temperature and humidity fluctuations from second- and third-order structure functions. *J. Fluid Mech.* **50**, 257.

PARK, J. T. 1976 Inertial subrange turbulence measurements in the marine boundary layer. Ph.D. thesis, University of California, San Diego.

STELLEMA, L., ANTONIA, R. A. & PRABHU, A. 1975 A constant current resistance thermometer for the measurement of mean and fluctuating temperatures in turbulent flows. *Charles Kolling Res. Lab., Dept. Mech. Engng, Univ. Sydney, Tech. Note* FD-12.

TAYLOR, R. J. 1958 Thermal structures in the lowest layers of the atmosphere. *Austr. J. Phys.* **11**, 168.

VAN ATTA, C. W. 1974 Influence of fluctuations in dissipation rates on some statistical properties of turbulent scalar fields. *Izv. Atmos. Ocean. Phys.* **10**, 712.

VAN ATTA, C. W. 1977 Effect of coherent structures on structure functions of temperature in the atmospheric boundary layer. *Arch. Mech.* **29**, 161.

VAN ATTA, C. W. & PARK, J. T. 1972 Statistical self-similarity and inertial subrange turbulence. In *Lecture Notes in Physics*, vol. 12. *Statistical Models and Turbulence* (ed. M. Rosenblatt & C. W. Van Atta), p. 402. Springer.

YAGLOM, A. M. 1949 On the local structure of a temperature field in a turbulent flow. *Dokl. Akad. Nauk S.S.S.R.* **69**, 743.

YEH, T. T. 1971 Spectral transfer and higher-order correlations of velocity and temperature fluctuations in heated grid turbulence. Ph.D. thesis, University of California, San Diego.